Preprint typeset in JINST style - HYPER VERSION

Measurement of electromagnetic shower densities at very high granularity

R. Coath[a], D. Cussans[b], J. P. Crooks[a], P. D. Dauncey[c,*], R. Gao[d], J. Goldstein[b], A.-M. Magnan[c], Y. Mikami[e,†], M. Noy[c,‡], A. Nomerotski[d], T. Price[e], V. Rajovic[e,§], M. Stanitzki[a], J. Strube[a], R. Turchetta[a], M. Tyndel[a], J. J. Velthuis[b], N. K. Watson[e], J. A. Wilson[e], Z. Zhang[a]

[a] *STFC, Rutherford Appleton Laboratory, Chilton, Didcot, UK.*
[b] *School of Physics, University of Bristol, Bristol, UK.*
[c] *Department of Physics, Blackett Laboratory, Imperial College London, London, UK.*
[d] *Department of Physics, University of Oxford, Oxford, UK.*
[e] *School of Physics and Astronomy, University of Birmingham, Birmingham, UK.*

E-mail: P.Dauncey@imperial.ac.uk

ABSTRACT: We present measurements of the charged particle densities in electromagnetic showers as a range of shower energies and converter thicknesses. Relevance to DECAL. By modelling the detector response carefully with single particles, the densities are compared with simulation and reasonable agreement is observed.

KEYWORDS: Calorimeter methods, Detector modelling and simulations, Solid state detectors.

*Corresponding author

†Current address: Institut Pluridisciplinaire Hubert CURIEN, 23 rue du loess - BP28, 67037 Strasbourg CEDEX 2, France.

‡Current address: CERN, CH-1211 Genève 23, Switzerland.

§Current address: Faculty of Electrical Engineering, University of Belgrade, Bulevar kralja Aleksandra 73, 11120 Belgrade, Serbia.

Contents

1. Introduction

DECAL concept described elsewhere [1]. Sensors developed for this application [2], [3]. Main uncertainty due to lack of very high granularity shower data.

Current paper describes first measurements of EM showers with a highly granular detector. Data taken at CERN HB6 North Area beam in Sept 2010. Data takes consisted of positive hadrons with momentum of 120 GeV and positrons with momenta from 10 to 100 GeV. Detector used was EUDET telescope with tungsten inserted between the planes of sensors to produce EM showers.

In the rest of this paper, section 2 contains a description of the equipment used for these measurements. Section 3 describes the performance of the telescope with single charged particles. It also gives details of the simulation developed for the sensor response. The data taken with electromagnetic showers are described in section 4, which includes a comparison of the shower densities with simulation. Finally, section 5 gives the conclusions from these studies.

2. The EUDET telescope

The EUDET telescope is a six-layer silicon sensor device which is available as a multi-purpose facility. The telescope was developed as part of the EUDET project [4] and details of the telescope design can be found in [5]. A description of the main features of the telescope relevant to this paper are given below.

2.1 Sensors

MIMOSA-26 CMOS pixel sensors [6]. Fabricated with 0.35 μm AMS process. Thickness of 700 μm (CHECK!) with 15 μm epitaxial layer. Pixel regular array of 1152×576 pixels with a pixel pitch of 18.4 μm, giving a total active area of $21.1 \times 10.6\,\mathrm{mm}^2$. Readout is performed using a rolling shutter with a frame period of 110 μs and for each event, data from two contiguous full rolling shutter frames are kept. For the studies presented here, no selection is made using the frame time so hits from the full two frames are used.

EPI LAYER UPSTREAM OR DOWNSTREAM?

2.2 Telescope layout

Two arms, each of three sensors. Sensors in the two arms spaced XXX mm apart. Space between two arms was set to the minimum of YYY mm. This was as close as was possible, given the mechanical structure of the telescope.

Triggering was performed using two scintillators, each $2 \times 1\,\mathrm{cm}^2$, and hence matched to the sensor size, and 3 mm thick. These were mounted mounted 6 mm in front of the first sensor. The trigger required both scintillators to fire at the same time. Two other scintillators were mounted behind the back telescope arm. These were not included in the trigger requirement for any of the data taken as this would have required rear leakage for the shower data and hence would have led to a bias.

A tungsten stack for creating electromagnetic showers was optionally inserted between the two arms. The stack was made of a number of plates of tungsten, each $5 \times 5\,\mathrm{cm}^2$ wide and 3 mm thick. This size was significantly larger than the sensors and so could be easily placed to cover the full active region of the telescope without requiring accurate alignment. Tungsten radition length $X_0 = 3.5$ mm so each plate corresponds to $0.86X_0$. The tungsten plates were held in place by an aluminium support made of a sheet of aluminium 1 mm thick. This was in place for all data taken, even when no tungsten sheets were present. The aluminium support and its mount were mechanically separate from the telescope arm mounts. This allowed the tungsten sheets to be inserted and removed without causing a major disturbance to the sensor alignment.

Figure 1 shows the layout of the apparatus in the beam line. The z axis was defined to be along the nominal beam direction and the y axis was vertically up, with the x axis defined to form a right-handed coordinate system. The x and y coordinates were defined to be centred on the most upstream sensor of the telescope (layer 0) while $z = 0$ was defined as the downstream surface of the aluminium mount, which was equivalent to the upstream face of the tungsten stack when tungsten sheets were present.

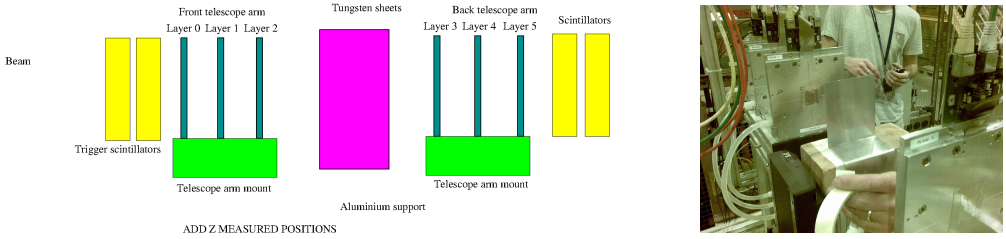

Figure 1. *Left: Schematic diagram of the layout of the telescope sensors, scintillators and tungsten sheets (not to scale). The z coordinates are shown in mm and the layer numbering defines the convention used in this paper. Right: Photograph of the telescope viewed from upstream. The last of the front arm sensor boxes and all three of the back arm sensors boxes are visible. The thin aluminium window indicating the position of the sensor within the box is also visible for the first back telescope box, layer 3. The tungsten stack aluminium support is shown between the arms. No tungsten sheets were present at the time of the photograph.*

2.3 Data acquisition

The readout is digital, so each pixel reports either a hit or not. Data taken with several thresholds. Programmable in arbitrary units; data taken with values between 6 and 10.5 units.

2.4 Data taken

Beam data were taken with positive hadrons and with positrons. The hadron data were all taken with a beam momentum of 120 GeV, for which the beam mainly consists of pions. All the hadron data used for this analysis were taken with no tungsten inserted within the telescope.

The beam ws delivered in 10 s spills with a period of 45 s. For the 120 GeV hadron beam, the intensity was high enough that the event rate was limited by the telescope DAQ rate. This was approximately 700 Hz within the spill and hence around 160 Hz on average. The event size for these events was on average 1 kByte per event. The total amount of hadron beam data taken was 1.3 million events.

The positron data were taken with beam momenta between 10 and 100 GeV and with the amount of tungsten varied between 0 and 16 sheets, equivalent to 0 to $14X_0$. In contrast to the hadron beam, the positron beam was much less intense, particularly for low momentum. This limited the event rate, giving average rates as low as 10 Hz at 10 GeV. Due to showering in the tungsten, the event sizes were larger than for the hadron data, varying between 1 and 2 kBytes per event, depending on the configuration. Table 1 shows the numbers of events taken for each combination of beam energy and tungsten thickness. A total of 2.2 million positron events were taken.

3. Single track measurements

The telescope alignment and tuning of the simulation model were done using the hadron beam data taken at 120 GeV. Cross checks of the sensor modelling were done with the hadron data and also the 100 GeV positron data. Tungsten sheets were not present for the data used for these studies. The hadron data were taken interspersed between the positron data runs throughout the beam period.

Table 1. *Numbers of positron beam events (in thousands) taken for each combination of tungsten sheets/thickness (in radiation lengths) and beam momentum (in GeV).*

Tungsten		Beam Momentum					
Sheets	Thickness (X_0)	10 GeV	20 GeV	40 GeV	60 GeV	80 GeV	100 GeV
0	0.0				50		48
2	1.7			31	61	81	102
4	3.4	22	19	40	70	100	106
6	5.1	5	17	26	60	62	58
8	6.9	9	24	35	53	84	101
10	8.6	11	20	29	60	82	92
12	10.3	13	23	30	61	84	102
14	12.0		31	31	61	81	102
16	13.7						104

Sum over two rolling shuttle frames. Clusters formed from all pixels above threshold which at adjacent to each other, both along a side or at a corner.

3.1 Alignment

The telescope sensors were aligned to each other using the beam data. Their nominal positions were defined to have the centre of the sensor active area at $x = y = 0$ and have the pixel edges along the x asnd y axes. For alignment, a horizontal (Δx) and vertical (Δy) offset from nominal, and an x-y rotation angle (α) were determined for each sensor. The other possible geometric parameters (a z offset and non-perpendicularity of the sensors to the z axis) were neglected as they have a very small effect on the analysis.

Since there was no external reference, the most upstream sensor (layer 0) was defined to have $\Delta x = 0$, $\Delta y = 0$ and $\alpha = 0$, while the most downstream sensor in the front arm (layer 2) was defined to have fixed values of Δx, Δy and α such that the average reconstructed particle direction was parallel to the z axis. The remaining 12 alignment parameters, namely all three parameters for layers 1, 3, 4 and 5, were determined from reconstructed tracks. These alignment parameters were determined for each run independently and the method used depended on whether there were tungsten sheets installed within the telescope or not.

With no tungsten, then tracks were reconstructed using clusters from each of the six layers. The clusers were required to have at most four pixels so that the track hit position and error were well-defined. A chi-squared track fit was performed for all possible combinations of six clusters satisfying this requirement and consistent with the known beam angular divergence, with one cluster from each layer. The fit assumed an averaged cluster resolution of 3 μm. The track fit was to a straight line with no allowance for multiple scattering, as this was found to be negligible for the data with no tungsten (beam momentum of 60 GeV or higher). A initial approximate alignment determined by hand and a loose fit chi-squared selection allowed a set of clusters to be found which formed tracks. The alignment parameters were then varied to minimise the total fit chi-squared values, summed over all the tracks. This procedure was iterated several times until it converged.

For runs with tungsten, then forming tracks in all six layers is not reasonable. In these runs, then tracks are found using just the first three layers, with the same cluster and angular cuts as above. Since tracks are often formed in the back three layers by particles from the shower leaving the tungsten, then a similar procedure was used to find tracks using hits in the back three layers. In these runs, only the alignment of layers 1 and 4 could be determined by minimising the total track chi-squared value.

The alignment parameters were found separately for each beam run with at least 10 tracks. The results of the parameter fits are shown in figure 2 as a function of the run number. It was found that the alignment parameters were stable over the whole data-taking period to within 2 μm in x and y and 0.1 mrad in α for all layers. Small changes to the alignment below these levels were observed, corresponding to times when the tungsten stack was handled to change the number of sheets. The alignment was adjusted in a run-dependent fashion to allow for these shifts. The final alignment parameters used for the studies reported in this paper are also shown in figure 2.

3.2 Simulation model

The telescope material and particle interactions were modelled using the GEANT4 simulation package [7]. The sensor response to the simulated energy deposits was modelled as described below. This sensor response simulation was treated as a simplified effective parametrisation rather than a detailed physical model as this was found to give a sufficiently good description of the observed data.

The epitaxial thickness of 15 μm results in a most probable signal charge of around 1200e^- being generated in the sensors. This charge will diffuse within the sensor before being collected by the signal diode. A simple two-dimensional model of this process was used where the charge was assumed to diffuse according to a normalised Gaussian distribution centred on the initial charge deposit position, such that the fraction of the total charge collected by each pixel was the integral of the Gaussian over the area of the pixel. Any depth dependence within the epitaxial layer was ingored. A region of 5×5 pixels centred on the initially hit pixel was considered, as the diffusion spread was found to result in negligible signals in pixels outside this area. The width of the Gaussian was treated as a free parameter to be determined from data.

The sensor noise was modelled by adding an extra amount of signal charge to each pixel which had signal, according to a Gaussian distribution. The width of this noise Gaussian was also treated as a free parameter to be determined from the data. The pixels which were too far from the charge deposits to have signal were randomly chosen whether to have been above threshold according to a rate determined from the data.

The final parameter needed for the sensor simulation was the calibration of the arbitrary threshold unit to signal charge units. This parameter was again determined from the data.

3.3 Tuning simulation parameters

Used hadron data only. Most data were taken with threshold settings of 10 units for each layer, except layer 3 for which 9 units was used. However, for some specific runs, thresholds of 6, 8, 9, 10 and 10.5 units were used in all layers.

For each sensor layer being studied in turn, tracks were formed from clusters in the other five layers. As for the alignment study described previously, these were fitted with a straight line,

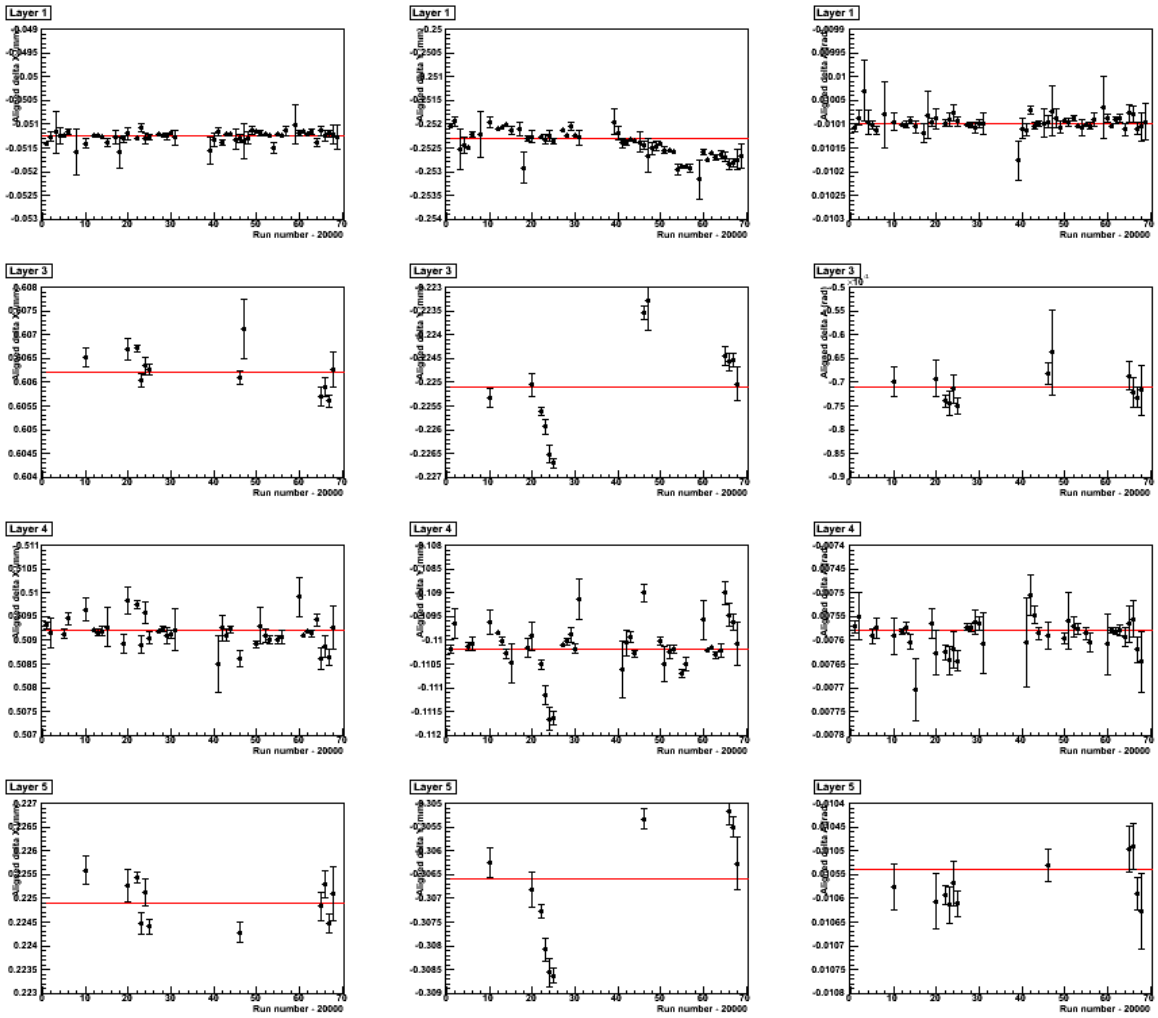

Figure 2. *Sensor alignment parameters as a function of run number. The plots show the values of Δx (left), Δy (centre) and α (right), for layers 1, 3, 4 and 5 (top to bottom) determined for each run, where applicable. The red lines show the values used for the alignment parameters in the following studies. SQUARE/CIRCLE FOR W/NO-W runs?*

neglecting multiple scattering effects, using an averaged cluster error of 5 μm. Tracks with a chi-squared probability of greater than 0.05 were projected into the layer being studied. PLOT OF DISTANCE TO NEAREST CLUSTER. SAME PLOT BUT WITH HALF-SENSOR OFFSET IN X AND Y TO SHOW NOISE RATE.

Any cluster within XXX μm of the track projection was considered to be due to the hadron. The number of tracks with no associated cluster gives an estimate of the sensor efficiency. This case is treated below as "zero-pixel" clusters. Although the same data were used for the alignment as for this analysis, there is no significant bias in this event-by-event track-cluster association as the alignment is an average over the whole dataset.

The associated clusters were characterised by their shapes. The pixel arrays were assumed to

be symmetric in terms of rotations by multiples of 90°, so that clusters which differed purely by their orientation were treated identically. Clearly, zero-pixel and one-pixel clusters have a unique shape, but all clusters formed from higher numbers of pixels have more than one possible shape. Figure **??** shows some of the most commonly occuring shapes, which account for over XX% of all clusters. The fractions of each of these ten (CHECK) most common cluster shapes (including zero-pixel clusters) was measured separately for each sensor layer and for each threshold value for which data were taken. An example of the fractions is shown in figure **??**.

Several simulated datasets were generated to model these events. The three sensor simulation parameters for each layer were each varied and a chi-squared formed between the shape fractions observed in the data compared with those predicted by the simulation. The set of three parameters which gave the best chi-squared match were found for each layer independently. The resulting optimal values are given in table **??**. It is seen that layer 3 has a significantly lower efficiency for a given threshold than the other five layers. For this reason, when taking the shower data described in section 4, this sensor was operated with a threshold of 9 units, while all other layers were operated with a threshold of 10 units.

3.4 Comparison of cluster positions

A cross-check of the parameter tuning can be made by estimating the particle impact locations within the pixel at which the various cluster shapes are likely to occur. For example, it would be expected simply from symmetry considerations that a two-pixel cluster would be most likely when the particle hits the pixel near the midpoint of an edge, while a four-pixel square cluster should be most likely for particles entering the pixel near its corner.

Figure **??** shows the positions of the simulated particles which give rise to the ten (CHECK) most common clusters. It is seen that the above expectations for two-pixel and four-pixel clusters are indeed true. Figure **??** shows the positions of the associated track projection within the pixel for each cluster shape from the simulation. The cluster positions are washed out due to the track projection resolution but the general effect is still visible. Finally, figure **??** shows the positions of the track projection within the pixel for data, which is seem to match well to the simulation within the available statistics.

3.5 Comparison of cluster resolutions

A second cross-check is possible by measuring the resolution of each cluster. The centre of each cluster is defined as the geometrical average of the pixels used to form the cluster, i.e. for a cluster with N pixels at positions $\vec{r}_i$, then the cluster position $\vec{r}_C$ is

$$\vec{r}_C = \frac{\sum_{i=1}^{N} \vec{r}_i}{N}$$

The differences of the centre of the clusters from the track projections for each cluster shape are shown in figure **??**. Done for two directions; sometimes symmetric, when not, then rotated to be same orientation in each case. The width of these distributions arises from both the track projection error and the cluster centre position error. The track fit allows an estimate of the projection error to be made which can be subtracted is quadrature to estimate the cluster position error. These values are shown in figure **??**; again, good agreement is shown between data and simulation for most cases.

3.6 Positron track data

Same plots but using positrons with no tungsten. It is seem that the cluster shape distributions are very similar.

Figure 3. *Typical pixel threshold scans for a pre-shape pixel.*

4. Electromagnetic shower measurements

EM showers were created in the EUDET telescope by inserting tungsten sheets between the two telescope arms. The positron data taken for each beam momentum and amount of tungsten were shown in table **??**. Clearly, with the tungsten only inserted in one position, and using sensors which are limited in size to around $2 \times 1\,\mathrm{cm}^2$, it is not possible to contain the shower and make an energy resolution measurement directly. The aim of this study is to measure the properties of the EM shower at very high granularity. In particular, the main aim was to measure the shower density as a function of the angle of the particles to the shower axis.

ERROR ON ANGLE DUE TO THICKNESS OF TUNGSTEN?

4.1 Measurement of shower density

The density of particles in an EM shower falls off rapidly with distance from the core of the shower. Therefore, to measure the density, it is essential to estimate the position of the shower axis event by event. To do this, the first arm, containing the first three layers of sensors, of the telescope were used. Tracks were constructed by requiring a cluster in each of the three layers with a chi-squared probability for the track fit of greater than 0.05. In this case, since beam momenta down to 10 GeV were used, multiple scattering effects are no longer negligible. To allow for this, the cluster position error in layer 0 was inflated by adding an extra term in quadrature of XXX/p_b, where p_b is the beam momentum.

EPI UPSTREAM OR DOWNSTREAM?

The selected events were also vetoed for early showering positrons by requiring the number of clusters in the first three layers to be within three standard deviations of the average number (CHECK). In addition, all combinations of the the remaining clusters in the first three layers after the track was reconstucted were used to try to find a second track. Any event with a second track satisfying a chi-squared probability for the track fit of greater than 0.01 were discarded (CHECK).

CONVERT POSITION TO ANGLE. INDEPENDENT MEASUREMENT FOR EACH LAYER. For the remaining events, the reconstructed track was projected onto each of the last three sensors in turn. The positions of all clusters in these layers was compared with the extrapolated track positions. The distribution of the distances between the cluster and track projection gives an estimate of the shower density as a function of the radial distance from the core of the shower.

Since the sensors are relatively small compared with the beam width, then it is possible to have showers close to the edge of the sensors, where many particles miss the sensors and so are unmeasured. A event by event correction must be made in order that the density is not biased

by such cases. For each event, the active sensor area available for measuring particles around the track projection was recorded as a function of the distance from the track projection. This gives a normalisation function with which to divide the observed cluster distribution so as to get a true cluster density as a function of distance from the track.

Figure **??** shows the distribution of this angle for the example case of the beam momentum of 100 GeV and $99.9X_0$ of tungsten as measured in layer 4. This distribution can be characterised by the peak height, which gives the core density at zero angle, and the width. The dependences of the peak height and width for all combinations of beam momentum and tungsten thickness are shown in figure **??**. It is seen that consistent results are obtained from all three sensor layers.

4.2 Comparison with simulation

Can only effectively measure charged particle contribution. Much lower rate of photon interactions with sensor.

GEANT4 EM SHOWER GENERATORS?

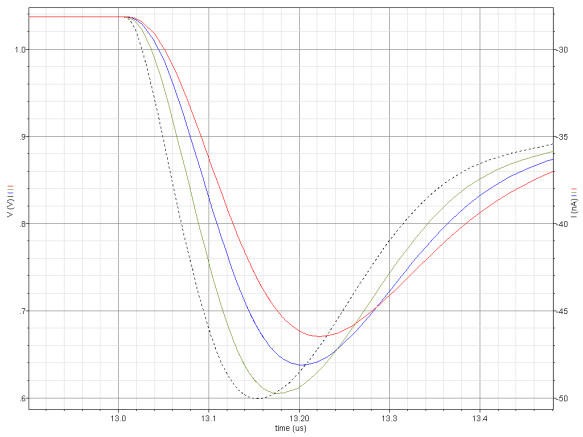

Figure 4. *Simulated reponse of pre-shape circuit to pulses of the same magnitude but with varying collection times. The pulse charge is injected at 13 µs on the time axis and collected with an exponential rise, with time constants of 0 ns (black, dashed), 25 ns (green), 50 ns (blue) and 75 ns (red). Zero corresponds to a diode interaction while a typical epitaxial interaction corresponds to the 50 or 75 ns curve.*

4.3 Track-independent method

Δr_{ij} for all pairs of clusters i and j. Independent of track reconstruction but sensitive to core density for small values of Δr. EXAMPLE PLOT; CHARACTERISE BY PEAK AND WIDTH. COMPARE WITH SIM.

5. Conclusions

Measurements of the core shower densities of electromagnetic showers have been made at very high granularity. Their dependence on energy and shower depth have been presented. Having

carefully modelled the sensor response, the simulation of showers shows good agreement with the densities measured in data.

The biggest uncertainty in estimating the performance of a future digital electromagnetic calorimeter has been the lack of measurements verifying the simulation at the small granularities required. The measurements presented here indicate that the simulation does a reasonable job, even at a granularity around a factor of two finer than being proposed for a digital calorimeter. Hence, these measurements have put the projections of digital calorimeter performance on a firmer footing.

Acknowledgments

This work was funded in part by the EU FP7 programme, via the EUDET infrastructure collaboration. We would like to thank the EUDET collaboration for their help, organisation and technical support during the beam tests. In particular, we are indebted to I.-M. Gregor for her assistance and E. Corrin and his help with the EUDET software, both during and after the beam period.

We would also like to thank the CERN beam delivery team for providing reliable and high quality beam throughout the period of our tests.

References

[1] J. A. Ballin *et al.*, *A MAPS-based Digital Electromagnetic Calorimeter for the ILC*, 2007 International Linear Collider Workshop (LCWS07 and ILC07), Hamburg, Germany (2007), and proceedings thereof, arXiv:0709.1346.

[2] P. D. Dauncey, *Performance of CMOS sensors for a digital electromagnetic calorimeter*, Proceedings of the 35th International Conference of High Energy Physics (ICHEP10), Paris, France (2010), `http://pos.sissa.it/archive/conferences/120/502/ICHEP 202010_502.pdf`.

[3] J. A. Ballin *et al.*, *Design and performance of a CMOS study sensor for a binary readout electromagnetic calorimeter*, *J. Inst.* **6** P05009, *doi:10.1088/1748-0221/6/05/P05009*, arXiv:103.4265.

[4] EUDET Collaboration, `http://www.eudet.org/`.

[5] EUDET Collaboration, E. Corrin, *The EUDET high resolution beam telescope - the final digital readout*, EUDET-Report-2009-06, IEEE Nuclear Science Symposium, Orlando, U.S.A. (2009), *Nucl. Sci. Symp. Conf. Rec. 2009 IEEE*, 816, *doi:10.1109/NSSMIC.2009.5402354*.

[6] J. Baudot *et al.*, *First test results of MIMOSA-26, a fast CMOS sensor with integrated zero suppression and digitized output*, IEEE Nuclear Science Symposium, Orlando, U.S.A. (2009), *Nucl. Sci. Symp. Conf. Rec. 2009 IEEE*, 1169, *doi:10.1109/NSSMIC.2009.5402399*.

[7] GEANT4 Collaboration, S. Agostinelli *et al.*, *Geant4 - a simulation toolkit*, *Nucl. Inst. Meth.* **A506** (2003) 250, *doi:10.1016/S0168-9002(03)01368-8*; J. Allison *et al.*, *Geant4 developments and applications*, *IEEE Trans. Nucl. Sci.* **53** (2006) 270, *doi:10.1109/TNS.2006.869826*.